NASA CONTRACTOR REPORT

A NUMERICAL SOLUTION FOR THE MINIMUM INDUCED DRAG, AND THE CORRESPONDING LOADING, OF NONPLANAR WINGS

by J. L. Lundry

Prepared by
THE MCDONNELL DOUGLAS CORPORATION
Long Beach, Calif.
for Langley Research Center

NATIONAL AERONAUTICS AND SPACE ADMINISTRATION • WASHINGTON, D. C. • NOVEMBER 1968

NASA CR-1218

A NUMERICAL SOLUTION FOR THE MINIMUM INDUCED DRAG, AND THE CORRESPONDING LOADING, OF NONPLANAR WINGS

By J. L. Lundry

Issued by Originator as Report DAC-66900

Prepared under Contract No. NAS 1-7484 by
THE McDONNELL DOUGLAS CORPORATION
Long Beach, Calif.

for Langley Research Center

NATIONAL AERONAUTICS AND SPACE ADMINISTRATION

For sale by the Clearinghouse for Federal Scientific and Technical Information
Springfield, Virginia 22151 – CFSTI price $3.00

A NUMERICAL SOLUTION FOR THE MINIMUM INDUCED DRAG, AND THE CORRESPONDING LOADING, OF NONPLANAR WINGS - FINAL REPORT

By J. L. Lundry

The McDonnell Douglas Corporation

ABSTRACT

A numerical procedure has been developed for the accurate computation of the minimum induced drag, and the associated loading, of nonplanar wings. The minimum induced drag and the loading are determined by the solution of a potential problem about the shed vortex wake in the Trefftz plane. The potential problem is analyzed in an auxiliary mapping plane that is related to the physical plane by the Schwarz-Christoffel transformation; the procedure can therefore be applied to configurations with front views that can be approximated by straight line segments. The success of the method depends on an iteration that converges satisfactorily for most cases. Comparisons of results of the method with results of known test cases show that errors in the minimum induced drag and in the corresponding loading are of the order of 10^{-4} when the method is programmed in single precision arithmetic for an IBM 7094.

A NUMERICAL SOLUTION FOR THE MINIMUM INDUCED DRAG, AND THE CORRESPONDING LOADING, OF NONPLANAR WINGS - FINAL REPORT

by J. L. Lundry

The McDonnell Douglas Corporation

SUMMARY

A numerical procedure has been developed for the accurate computation of the minimum induced drag, and the associated loading, of nonplanar wings. The minimum induced drag and the loading are determined by the solution of a potential problem about the shed vortex wake in the Trefftz plane. The potential problem is analyzed in an auxiliary mapping plane that is related to the physical plane by the Schwarz-Christoffel transformation; the procedure can therefore be applied to configurations with front views that can be approximated by straight line segments. Previously, the main computational difficulty with this approach was the determination of the mapping constants. Two methods to obtain these constants are presented. By means of the rheoelectric analogy to potential flow, the mapping constants can be measured with an analog field plotter. The measured values contain small experimental errors, and are used as initial values for an iteration that determines the mapping constants accurately. The mapping derivative is integrated numerically to obtain an approximate Trefftz-plane geometry; deviations of this geometry from the desired Trefftz-plane geometry are used to calculate corrections to the mapping constants.

Alternatively, the mapping constants can be determined without resorting to analog experimentation by evaluating them for a series of geometrically related configurations that ends with the desired configuration. The mapping constants for each member of the series are used as the equivalent of experimental values for the next member of the series, whose mapping constants can then be determined with the iteration scheme employed in the experimental method. The series starts with the monoplane degenerate equivalent of the desired configuration, for which the mapping constants are known. This procedure is successful if each member of the series differs geometrically from its neighbors by a small amount.

Once the mapping constants are known, the minimum induced drag and the associated loading are determined by quadrature.

The procedure has been applied to seven nonplanar lifting configurations, resulting in the development of Computer Program 55VD in the FORTRAN IV language for use on an IBM 7094. Program 55VD has been converted to FORTRAN 2.0 for use on the Langley Research Center's CDC 6000 series digital computers. This report summarizes the development of Computer Program 55VD.

INTRODUCTION

To increase aircraft efficiency, the use of existing aircraft components to lower induced drag is being considered. Such components include pylons, engines, fences, and other surfaces that can support the aerodynamic loads required for minimum induced drag. Nonplanar lifting configurations that produce minimum induced drag can be studied in three steps:

(1) For a given configuration (wing alone, wing with end plates, etc.), determine the shed vorticity distribution to minimize induced drag for a specified lift.

(2) Given (1), compute the minimum induced drag.

(3) Given (1), compute the geometry (camber and/or twist) to produce the minimum induced drag loading.

This report deals with steps (1) and (2) for a series of nonplanar wings with varying arrangements of auxiliary lifting surfaces (i.e., pylons, fences, and end plates) by applying Munk's theory of minimum induced drag.

Munk's Theory

In Reference 1, Munk develops a theory for the minimum induced drag, and the associated loading, of arbitrary lifting configurations. All loadings are assumed light, so that velocity perturbations are small and the vortex wake in the Trefftz plane may be assumed undistorted. The loadings can be projected onto a plane normal to the free-stream velocity without changing the induced drag of the lifting system (Stagger Theorem). Munk's criterion for minimum induced drag is illustrated in Figure 1, and requires the induced velocity normal to the projected loadings to be proportional to the cosine of the angle of lateral inclination of the projected loadings. Munk further demonstrates that the loading to satisfy this criterion can be found by solving a potential flow problem about the vortex wake in the Trefftz plane, in which the undisturbed flow is parallel to the downwash. The required loading is locally proportional to the potential difference across the wake and is normal to the wake.

Applications of Munk's Theory

Munk applies his theory to the monoplane, and obtains the classic result that a constant downwash across the span produces the minimum induced drag

$$D = \frac{L^2}{4 \pi q s^2} \qquad (1)$$

and is given by an elliptical distribution of load. In References 2-6, the theory is applied analytically to nonplanar configurations consisting of either combinations of a monoplane with vertical fences or a wing with part-span or full-span dihedral. In Reference 7, the rheoelectric analogy to potential flow is exploited to determine experimentally loadings that

satisfy Munk's criterion for complex nonplanar lifting configurations; the lift and the minimum induced drag are then evaluated numerically. Unfortunately, the numerical results of this method can contain significant errors as shown by Reference 8.

Reference 8 obtains a solution to the potential problem in an auxiliary mapping plane related to the real (Trefftz) plane by the Schwarz-Christoffel transformation for configurations with front views that may be approximated by straight line segments. Previously, the main computational difficulty with this approach was the determination of the mapping constants. By means of the rheoelectric analogy to potential flow, the mapping constants can be measured with an analog field plotter. The measured values of the mapping constants contain small experimental errors, and are used as initial values for an iteration that determines the mapping constants accurately. An approximate Trefftz-plane geometry is obtained by numerical integration of the mapping derivative; deviations of this geometry from the desired Trefftz-plane geometry are used to calculate corrections to the mapping constants. Once the mapping constants are known, the minimum induced drag is determined by quadrature. A digital computer program was required to obtain the numerical results of Reference 8.

This report incorporates the work of Reference 8 and describes the following extensions:

(1) Calculation of the loading on all surfaces to produce minimum induced drag for Configurations 1-7 (See Figure 2).

(2) Application of the numerical scheme of Reference 8 to the calculation of the minimum induced drag of Configurations 6 and 7. (The results of Reference 8 for Configurations 1-5 are included in this report).

(3) Development of an alternative method to determine the mapping constants so that the analog experiments could be eliminated from the method of Reference 8.

The extensions were funded under NASA contract NAS1-7484. A user's manual for the extended computer program and a detailed program description are provided as supplements to this report, and may be obtained upon request.[1]

The author wishes to acknowledge the contributions to this study of Prof. P.B.S. Lissaman of the California Institute of Technology. Prof. Lissaman has consulted frequently with the author since the start of this study.

- - - - - - - - -

[1]See request form at the back of this paper.

SYMBOLS

A,B,C,D, E,F,G,H,I	potentials in the real or physical plane (See Figure 3)
C_i	the i-th required geometry condition in the real plane
ΔC_i	error in C_i
D	minimum induced drag
I	the imaginary part of
L	lift
U	freestream velocity
a,b,c,d, e,f,g,h,i	potentials in the auxiliary plane (See Figure 3)
$\bar{e}$	the square root of the sum of the squares of the errors in the required geometry conditions: $$\bar{e} = \sqrt{\sum_{i=1}^{n} (\Delta C_i)^2}$$
$\bar{f}_i$	abscissa spacing parameter [See Equations (7) and (8)]
k	induced drag efficiency at minimum induced drag
ℓ	nondimensional length of auxiliary surface
n	number of required geometry conditions C_i
p_j	the j-th mapping constant or potential. The potentials are numbered in alphabetical order.
Δp_j	correction to p_j
q	dynamic pressure
s	semispan
$\bar{s}$	arc length
w_o	crossflow velocity
y	spanwise coordinate
z	complex variable in the real plane
Γ	dihedral angle in degrees
β	angle of lateral inclination (See Figure 1)

γ circulation (mean value is $\bar{\gamma}$ for each load-bearing surface)

ζ complex variable in the auxiliary mapping plane

η nondimensional semispan coordinate

ρ density

ϕ potential

ϕ_n normal derivative of ϕ

ANALYSIS

The basic theory for the minimum induced drag of nonplanar lifting configurations is given in Reference 1 and is described in the INTRODUCTION. A potential problem is formulated about the vortex wake in the Trefftz plane. The problem is analyzed numerically by the method of Reference 8 in an auxiliary mapping plane related to the Trefftz plane by the Schwarz-Christoffel transformation. First, the constants of the Schwarz-Christoffel mapping must be determined. The minimum induced drag can then be obtained by quadrature. Finally, the required load distribution can be obtained by interpolation. The seven general configurations sketched in Figure 2 are analyzed by Computer Program 55VD.

The Mapping Constants

Two methods to determine the mapping constants have been included in Program 55VD and are described here.

Rheoelectric Analog with Iterative Correction. By means of the rheoelectric analogy to potential flow, the mapping constants can be measured experimentally with an analog field plotter. The measured values of potential contain experimental errors, and are corrected by an iterative scheme that will be explained for Configuration 5. Figure 3 shows the Trefftz plane (also called real or physical plane) and the auxiliary mapping plane for Configuration 5. The Schwarz-Christoffel transformation between these planes is

$$\frac{dz}{d\zeta} = \frac{(\zeta - c)(\zeta - e)}{[(\zeta - a)(\zeta - b)(\zeta - g)]^{\frac{1}{2}}} (\zeta - d)^{\frac{\Gamma}{\pi} - \frac{1}{2}} (\zeta - f)^{-\frac{\Gamma}{\pi}} \qquad (2)$$

Given the experimental values of potential a, . . . , g, the geometry in the physical plane is evaluated by numerically integrating Equation (2). For example, the length $\overline{AB}$ is

$$\overline{AB} = z_B - z_A = \int_a^b \frac{dz}{d\zeta} \, d\zeta \qquad (3)$$

Each of the distances $\overline{AB}$, $\overline{BC}$, $\overline{CD}$, $\overline{DE}$, $\overline{EF}$, and $\overline{FG}$ in Figure 3 can be evaluated in this way, and each of the integrals has one or two integrable singularities at the end or ends of the integration interval. If an integral has two singularities, it is evaluated in two parts of equal range so that each numerical integral has at most one singularity. For example, the integral for the length $\overline{AB}$ has singularities at a and b, and is evaluated as

$$\overline{AB} = \int_{a}^{\frac{1}{2}(a+b)} \frac{dz}{d\zeta}\, d\zeta + \int_{\frac{1}{2}(a+b)}^{b} \frac{dz}{d\zeta}\, d\zeta \tag{4}$$

The first integral is singular at a in the form

$$\int_{a}^{\frac{1}{2}(a+b)} \frac{Z(\zeta)}{(\zeta - a)^{\frac{1}{2}}}\, d\zeta \tag{5}$$

and can be rewritten in the standard way as

$$\begin{aligned} &\int_{a}^{\frac{1}{2}(a+b)} \frac{Z(\zeta) - Z(a)}{(\zeta - a)^{\frac{1}{2}}}\, d\zeta + Z(a) \int_{a}^{\frac{1}{2}(a+b)} \frac{1}{(\zeta - a)^{\frac{1}{2}}}\, d\zeta \\ &= \int_{a}^{\frac{1}{2}(a+b)} \frac{Z(\zeta) - Z(a)}{(\zeta - a)^{\frac{1}{2}}}\, d\zeta + 2\, Z(a)\, [\tfrac{1}{2}(b - a)]^{\frac{1}{2}} \end{aligned} \tag{6}$$

The integrand $[Z(\zeta) - Z(a)]/[\zeta - a]^{\frac{1}{2}}$ is evaluated on the integration interval at up to fifty points that are spaced more closely near the singularity, and a modified Simpson rule is used to perform the quadrature. If the singularity is located at the lower end of the integration interval, the abscissa spacing is given by

$$\Delta\zeta_i = \frac{\bar{f}_i \left(\zeta_u - \zeta_e + \sum_{j=1}^{i-1} \Delta\zeta_j \right)}{m - i + 1} \tag{7}$$

where m is the number of intervals, $\bar{f}$ is given by

$$\bar{f}_{i+1} = 2\, \bar{f}_i \tag{8}$$

subject to the limitation $\bar{f}_i \leq 1$ with $\bar{f}_1 = 0.01$, and ζ_u and ζ_e are the upper and lower limits of the numerical integral. An analogous spacing of abscissae relative to the singularity is used if the singularity is located at the upper limit.

For the example of Configuration 5, the mapping derivative contains seven unknown constants. Six of these constants are independent (one must be fixed to define a coordinate origin) and determine the six lengths $\overline{AB}$, $\overline{BC}$, $\overline{CD}$, $\overline{DE}$, $\overline{EF}$, and $\overline{FG}$ in Figure 3. For practical reasons, the experimental values of the mapping constants are scaled linearly before they are used to evaluate the geometry in the real plane; this linear scaling changes only the absolute scale in the real plane and is equivalent to fixing one of the six independent mapping constants. For Configuration 5, the coordinate origin and the linear scaling are defined by setting b = 0 and e = 1. Five of the unknown mapping constants are used as the independent variables in a linear iteration scheme that is designed to satisfy the five required geometry conditions:

1) The fence must close ($\overline{BC} = \overline{CD}$).

2) The inboard wing must close ($\overline{AB} = \overline{FG}$).

3) The outboard wing must close ($\overline{DE} = \overline{EF}$).

4) The fence must have the proper length ($\overline{BC} = \ell[\overline{AB} + \overline{DE} \cos \Gamma]$).

5) The fence must have the proper semi-span location ($\overline{AB} = \eta[\overline{AB} + \overline{DE} \cos \Gamma]$).

The initial values of the mapping constants are measured experimentally with an analog field plotter. The corrections to the mapping constant Δp_j are computed from

$$-\Delta C_i = \frac{\partial C_i}{\partial p_j} \Delta p_j \qquad (9)$$

where ΔC_i is the error in C_i, the i-th geometry requirement. The 5x5 correction matrix $\partial C_i/\partial p_j$ is evaluated numerically by perturbing p_j slightly, scaling the potentials linearly if p_j is either b or e, and calculating the derivative as though C_i varies linearly with p_j. For Configuration 5, the potentials a, b, d, e, and g were selected from the seven unknown values of potential as the independent variables for the iteration. This simple iteration scheme converges rapidly for properly chosen independent variables. For some of the seven configurations, the set of mapping constants selected initially as independent variables did not give convergence, and other sets were chosen. However, convergence of the iteration scheme has been achieved for each of the seven configurations considered to date.

The preceding paragraphs describe the iteration that determines accurately the mapping constants for Configuration 5. Similar iterative schemes determine the mapping constants for Configurations 1-4, 6, and 7. Listed in Tables I and II are the parameters of significance to the iteration that vary with configuration. Table I presents the Schwarz-Christoffel mapping derivative, a definition of the linear scaling in the auxiliary mapping plane, and a list of the mapping constants used as independent variables in the iteration. Table II presents the required geometry conditions in the real plane for each of the seven configurations.

Table I

Mapping Derivative, Definition of Linear Scaling, and Independent Variables in Iteration Scheme

Configuration Number (See Figure 2)	Schwarz - Christoffel Mapping Derivative $\frac{dz}{d\zeta}$	Definition of Linear Scaling	Independent Variables
1	$\frac{(\zeta - c)(\zeta - e)}{[(\zeta - a)(\zeta - b)(\zeta - d)(\zeta - f)]^{\frac{1}{2}}}$	a = o, e = 1	a,b,d,f
2	$\frac{(\zeta - c)(\zeta - f)(\zeta - h)}{[(\zeta - a)(\zeta - b)(\zeta - d)(\zeta - e)(\zeta - g)(\zeta - i)]^{\frac{1}{2}}}$	d = o, g = 1	a,b,d,e,f,g,h
3	$\frac{(\zeta - b)(\zeta - e)}{[(\zeta - a)(\zeta - c)(\zeta - d)(\zeta - f)]^{\frac{1}{2}}}$	c = o, e = 1	b,d,e,f
4	$\frac{(\zeta - c)(\zeta - e)(\zeta - g)}{[(\zeta - a)(\zeta - b)(\zeta - d)(\zeta - f)(\zeta - h)(\zeta - i)]^{\frac{1}{2}}}$	d = o, g = 1	a,b,c,e,g,h,i
5	$\frac{(\zeta - c)(\zeta - e)(\zeta - d)^{\frac{\Gamma}{\pi} - \frac{1}{2}} (\zeta - f)^{-\frac{\pi}{\Gamma}}}{[(\zeta - a)(\zeta - b)(\zeta - g)]^{\frac{1}{2}}}$	b = o, e = 1	a,b,d,e,g
6	$\frac{(\zeta - c)(\zeta - f)}{[(\zeta - a)(\zeta - b)(\zeta - d)(\zeta - h)]^{\frac{1}{2}}} \left(\frac{\zeta - e}{\zeta - g}\right)^{\frac{\Gamma}{\pi}}$	b = o, f = 1	a,b,d,e,f,g
7	$\frac{(\zeta - d)(\zeta - e)(\zeta - g)^{\frac{1}{2}}}{[(\zeta - a)(\zeta - b)(\zeta - c)(\zeta - f)(\zeta - h)]^{\frac{1}{2}}}$	a = o, e = 1	b,c,d,f,g,h

Table II

Required Geometry Conditions in Trefftz Plane

Refer to Figure 2

Config. Number	Required Condition C_i						
	i = 1	i = 2	i = 3	i = 4	i = 5	i = 6	i = 7
1	$\overline{BC}=\overline{CD}$	$\overline{AB}+\overline{DE}=\overline{EF}$	$\overline{AB}= \eta\overline{EF}$	$\overline{BC} = \ell\ \overline{EF}$			
2	$\overline{BC}=\overline{CD}$	$\overline{EF} = \overline{FG}$	$\overline{AB}+\overline{DE}+\overline{GH}=\overline{HI}$	$\overline{AB} = \eta_i\overline{HI}$	$\overline{AB} + \overline{DE} = \eta_o\ \overline{HI}$	$\overline{BC} = \ell_i\ \overline{HI}$	$\overline{EF} = \ell_o\ \overline{HI}$
3	$\overline{AB}=\overline{BC}$	$\overline{DE} = \overline{EF}$	$\overline{CD} = \ell_H\ \overline{AB}$	$\overline{DE} = \frac{s_H}{s}\ \overline{AB}$			
4	$\overline{BC}=\overline{CD}$	$\overline{FG} = \overline{GH}$	$\overline{AB}+\overline{DE}=\overline{EF}+\overline{HI}$	$\overline{AB} = \eta_i(\overline{AB} + \overline{DE})$	$\overline{HI} = \eta_o(\overline{EF} + \overline{HI})$	$\overline{BC} = \ell_i(\overline{AB} + \overline{DE})$	$\overline{FG}=\ell_o(\overline{AB}+\overline{DE})$
5	$\overline{AB}=\overline{FG}$	$\overline{BC} = \overline{CD}$	$\overline{DE} = \overline{EF}$	$\overline{CD} = \ell(\overline{AB}+\overline{DE}\ \cos\Gamma)$	$\overline{AB} = \eta(\overline{AB}+\overline{DE}\cos\ \Gamma)$		
6	$\overline{AB}+\overline{DE}=\overline{GH}$	$\overline{BC} = \overline{CD}$	$\overline{EF} = \overline{FG}$	$\overline{AB}=\eta_i(\overline{GH}+\overline{FG}\ \cos\ \Gamma)$	$\overline{GH}=\eta_o(\overline{GH}+\overline{FG}\ \cos\ \Gamma)$	$\overline{BC}=\ell(\overline{GH}+\overline{FG}\ \cos\ \Gamma)$	
7	$\overline{AB}=\overline{GH}$	$\overline{BC} = \overline{FG}$	$\overline{DE} =\overline{CD} + \overline{EF}$	$\overline{BC} = \ell\ \overline{AB}$	$\overline{CD} = \ell_i\ \overline{AB}$	$\overline{EF} = \ell_o\ \overline{AB}$	

Successive Solution Scheme. A numerical method has been developed to determine the unknown constants of the Schwarz-Christoffel mapping without resorting to rheoelectric analog experimentation. The mapping constants are determined for a series of geometrically related configurations that ends with the desired configuration. The final values of the mapping constants for each member of the series are used as initial values for the next member of the series, whose mapping constants can then be determined with the iteration scheme developed for the rheoelectric analog method. The series is started with the monoplane degenerate equivalent of the desired configuration, for which the mapping constants can be determined from the solution for potential about a monoplane that is given in Reference 9.

The successive solution scheme has been applied to Configurations 1-7 of Figure 2, and operates successfully for Configurations 1-6 if each member of the series of related configurations differs geometrically from its neighbors by a small amount. However, the iteration for the mapping constants usually does not converge for Configuration 7 if the parameters ℓ, ℓ_i, and ℓ_o of Figure 2 are small. Therefore, the monoplane starting solution is replaced in the successive solution scheme by a solution for Configuration 7 with $\ell = 0.04$ and $\ell_i = \ell_o = 0.01$. The successive solution scheme operates successfully for Configuration 7 if values of the desired geometry are larger than those of the starting solution configuration; the scheme is usually unsuccessful if the desired geometry parameters are significantly smaller than those of the starting solution. The supplements to this report describe in detail the known limitations of the successive solution scheme for Configurations 1-7.

The Minimum Induced Drag

Once the mapping constants are known, the minimum induced drag is calculated in the terms of the efficiency k, where

$$D = \frac{L^2}{4 \pi s^2 q k} \tag{10}$$

In terms of the crossflow potential in the Trefftz plane,

$$L = \rho U \int \Delta \varphi dy \tag{11}$$

and

$$D = \frac{1}{2} \int \varphi \varphi_n d\bar{s} \tag{12}$$

the appropriate integrals being taken about the wake. Munk's criterion for minimum induced drag is

$$\varphi_n = w_o \cos \beta \tag{13}$$

so the minimum induced drag efficiency becomes

$$k = \frac{1}{\pi s^2 w_o} \int \Delta \varphi dy \tag{14}$$

If the expression for k is transformed into the auxiliary mapping plane for Configuration 5,

$$k = \frac{1}{\pi s^2} \; I \int_a^g \zeta \; \frac{dz}{d\zeta} \; d\zeta \qquad (15)$$

where I means "the imaginary part of". The integration is performed numerically with the technique used to evaluate the geometry integrals similar to the integral of Equation (3). However, Equation (15) does not need to be integrated numerically over the entire interval from a to g to evaluate k for Configuration 5. The interval is divided into regions identical to those used to evaluate geometry in the real plane. The integrals for regions that correspond to vertical sections of the vortex wake are zero, since Munk's criterion (Figure 1) specifies zero velocity normal to such sections. Similar regions occur in the integrals that evaluate k for the other configurations of Figure 2.

The Loading to Produce Minimum Induced Drag

Once the mapping constants are known, the potential may be computed in the physical plane as a function of geometric location. The required loading is proportional to the potential difference across the Trefftz-plane vortex wake.

Since the complex potential is conserved between the real plane and the auxiliary mapping plane, the potential is identical at corresponding points of the mapping. In the example of Figure 3, A = a, B = b, etc. When the distances in the real plane are calculated during the last cycle of the iteration that determines the mapping constants, the numerical parts of the integrals are stored in tabular form as a function of abscissa for the integration regions. The tabular results of the numerical integrations are modified to obtain a quantity proportional to potential in the real plane. For the first part of the interval A to B in the example of Figure 3,

$$z' - z_A = \int_a^{\zeta'} \frac{dz}{d\zeta} \; d\zeta$$

$$= \int_a^{\zeta'} \frac{Z(\zeta) - Z(a)}{\sqrt{\zeta - a}} \; d\zeta + 2 \, Z(a) \; \sqrt{\zeta' - a} \qquad (16)$$

where $\zeta' \leq \frac{1}{2}(a + b)$. The first term on the right side of Equation (16) is the quantity computed and stored during the calculation of the first part of the distance $\overline{AB}$ [See Equations (2) - (6)]. To this term must

be added only the second term of the right side of Equation (16) to obtain coordinates in the real plane as a function of corresponding ζ. A quantity proportional to the potential difference across the vortex wake in the real plane is obtained by interpolation in the tables of Z as a function of ζ. For each surface, the local loading is nondimensionalized with respect to the gross load.

COMPUTER PROGRAM 55VD

Computer Program 55VD has been written in the FORTRAN IV language for use on an IBM 7094 digital computer, and has been converted to FORTRAN 2.0 for use on the Langley Research Center's CDC 6000 series computers. Figure 4 presents the overall logic of Program 55VD. In several subroutines, internal logic is used to transfer to coding associated with the configuration being considered; such logic is not shown in Figure 4. Computing time per case varies from 0.1 minute to 3 minutes with an IBM 7094, depending on which of seven configurations is being analyzed, the number or ordinates used in the evaluation of the geometry and drag numerical integrals, and the rate of convergence of the iteration for the mapping constants. The main program and the twenty-four subroutines of Program 55VD are written on roughly 3700 FORTRAN source cards.

NUMERICAL RESULTS

To date, Computer Program 55VD has been used principally to substantiate the method and to determine its important limitations. The parameter k is presented in Figures 5-10 for a modest range of the geometric parameters of Configurations 1-5. Examples of load distributions for minimum induced drag are presented in Figures 11-19. For wings with end plates, Figures 11 and 12 compare exact loadings from Reference 4 with loadings from Computer Program 55VD for Configurations 1 and 4, respectively. Similar comparisons with results of Reference 6 are made in Figures 13 and 14 for Configuration 4. In each comparison, the results agree closely, although the geometry analyzed by Computer Program 55VD for each comparison is not identical to the geometry analyzed by the referenced methods. A precise comparison cannot be presented because of the limitations of Computer Program 55VD that are discussed in the supplements to this report.

Another example of the loading for minimum induced drag is presented in Figure 15 for Configuration 2. With the plotting scale of Figure 15, the loadings on the inboard fence and the outboard fence coincide. In Figures 16, 17, 18, and 19, examples of the loading corresponding to minimum induced drag are presented for Configurations 3, 5, 6, and 7, respectively.

DISCUSSION OF EXPERIMENTS ON NONPLANAR WINGS

References 10-21 report the results of experiments designed to determine the induced drag and stability characteristics of nonplanar wings. Most of the models are wings with end plates. These experiments are uniformly disappointing as minimum induced drag is not obtained. None of the models are designed properly for minimum induced drag even though induced drag is the principal concern of most of the experiments. None of the model wings of References 10-21 are twisted or cambered to produce the proper loading for minimum induced drag, although Reference 10 reports experiments with varying wing twist. Only References 15 and 21 report experiments on models with cambered end plates, and the loading for minimum induced drag is not described as the reason for choosing the camber in either reference. None of the end plates are twisted. Only the authors of References 10 and 18 specifically recognize that their models are not designed to carry the loading for minimum induced drag. The absence of such data in the literature is possibly due to incorrect extensions of the crossflow barrier explanation of end plate effects. In a two-dimensional airfoil test, the wind tunnel walls act as fully effective barriers to the crossflow about the wing tips, and induced drag is eliminated as a result. In an analogous way, end plates function as partially effective barriers to the crossflow, and reduce induced drag. The barrier concept apparently leads to the supposition that end plate planform is of prime importance to end plate effectiveness. References 10, 11, 13-16, 19, and 21 each contain experimental data for more than one end plate planform, and Reference 16 reports results of tests on fifteen end plate planforms. Reference 21 presents an "optimum" end plate planform design that attempts to minimize end plate friction drag for a given end plate effectiveness; the crossflow barrier explanation is the basis of the analysis. To be sure, a change of end plate planform is likely to produce a change of induced drag because the planform change alters the loading on both the end plate and the wing. Nevertheless, the end plate planform has no significance to minimum induced drag as long as the end plate and the wing can develop the loading for minimum induced drag. To reduce end plate friction drag, the end plate chord can be minimized, subject to the loading constraint. Once the loading and the planform geometry are known, the twist and/or camber to produce the loading must be calculated for both the wing and the end plates. For the general nonplanar lifting configuration, the proper loading and the twist and/or camber must be calculated for all load-bearing surfaces. In References 22 and 23, methods are discussed for calculating the twist of nonplanar configurations if the loading is specified.

Described in Reference 18 is an interesting use of end plates to improve overall aircraft performance. End plates are usually considered to be a means of reducing the drag of lifting aircraft, and thereby improving aircraft performance in takeoff, climb, cruise, and loiter. However, some aircraft performance characteristics improve with increasing drag — for example, landing distance and equilibrium rate of descent. A variable geometry end plate is suggested in Reference 18 as a means of either decreasing or increasing the drag of a given wing. The end plate would be designed to produce minimum induced drag in the basic configuration. In the alternative configuration, trailing edge flaps on the end plate or a pivot for the entire end plate would be used to change substantially the loading on the end plate and the wing, and thereby greatly increase the drag of the aircraft. Experimental evidence is presented in Reference 18 to support this idea.

CONCLUSIONS

A numerical method has been developed to determine accurately the minimum induced drag, and the corresponding loading, of nonplanar wings. The method can be applied to configurations with front views that can be approximated by straight line segments. The success of the method depends on an iteration that converges satisfactorily for most cases. Comparisons of results of the method with results of known test cases show that errors in the minimum induced drag and in the corresponding loading are of the order of 10^{-4} when the method is programmed in single precision arithmetic for an IBM 7094.

One full-scale flight test and several wind tunnel tests on nonplanar lifting wings have been reviewed. None of the experiments produced minimum induced drag because none of the models were designed to carry the loading for minimum induced drag. Proper design must include the calculation of twist and/or camber of the wing and of the auxiliary load-bearing surfaces after the necessary loading is determined.

REFERENCES

1. Munk, Max M.: The Minimum Induced Drag of Aerofoils, NACA Report No. 121, 1921.

2. Mangler, W.: The Lift Distribution of Wings with End Plates, NACA TM No. 856, 1938 (Translated by J. Vanier from: Die Auftriebsverteilung am Tragflugel mit Endscheiben, Luftfahrtforschung, V. 14, No. 11, Nov. 20, 1937, pp 564-569).

3. Mangler, W.: Lift Distribution on Wings with Lateral Plates, Douglas Aircraft Company Report No. LB-33497, December, 1966 (Translated by G. deMontalvo from Luftfahrtforschung, V. 16, 1939, pp 219-228).

4. Falkner, V. M., and Darwin, C.: The Design of Minimum Drag Tip Fins, A.R.C. R&M 2279, 1945.

5. Kuchemann, D., and Kettle, D. J.: The Effect of End Plates on Swept Wings, A.R.C. CP104, June, 1951.

6. Weber, J.: Theoretical Load Distribution on a Wing with Vertical Plates, A.R.C. R&M 2960, March, 1954.

7. Cone, C. D., Jr.: The Theory of Induced Lift and Minimum Induced Drag of Nonplanar Lifting Systems, NASA Technical Report R-139, 1962.

8. Lundry, J. L., and Lissaman, P.B.S.: A Numerical Solution for the Minimum Induced Drag of Nonplanar Wings, AIAA J. of Aircraft, V. 5, No. 1, January-February, 1968.

9. von Karman, Th. and Burgers, J. M.: General Aerodynamic Theory - Perfect Fluids, Division E, Vol. II, p 138 of Aerodynamic Theory, W. F. Durand, Editor-in-Chief, Julius Springer 1934-36 and Dover Publications, 1963.

10. Reid, E. G.: The Effect of Shielding the Tips of Airfoils, NACA Report No. 201, 1925.

11. Hemke, P. E.: Drag of Wings with End Plates, NACA Report No. 267, 1927.

12. Hubert, J.: Model Experiments on Aerofoils with Various Degrees of Sweep Back With and Without End Plates (Translated by V. P. Akimoff), R.T.P. Translation No. 1816, British Ministry of Aircraft Production, 1937.

13. Bates, W. R.: Collection and Analysis of Wind-Tunnel Data on the Characteristics of Isolated Tail Surfaces With and Without End Plates, NACA TN 1291, 1947.

14. Riebe, J. M., and Watson, J. M.: The Effect of End Plates on Swept Wings at Low Speed, NACA TN 2229, 1950.

15. Wadlin, K. L., Fontana, R. E., and Shuford, C. L., Jr.: The Effect of End Plates, End Struts, and Depth of Submergence on the Characteristics of a Hydrofoil, NACA RM L51B13, April 12, 1951.

16. Riley, D. R.: Wind-Tunnel Investigation and Analysis of the Effects of End Plates on the Aerodynamic Characteristics of an Unswept Wing, NACA TN 2440, August, 1951.

17. Peterson, R. B.: The Effects of Circular End Plates on the Lift, Drag, and Pitching Moment at Subsonic and Supersonic Speeds on a Modified Triangular Wing Having an Aspect Ratio of 2, a Taper Ratio of 0.33, and a 45° Swept Leading Edge, NACA RM A53J14, March, 1954.

18. Clements, H. R.: Canted Adjustable End Plates for the Control of Drag, Aeronautical Engineering Review, Vol. 14, No. 7, July, 1955, p 40.

19. Lowry, J. G., and Vogler, R. D.: Wind-Tunnel Investigation at Low Speeds to Determine the Effect of Aspect Ratio and End Plates on a Rectangular Wing with Jet Flaps Deflected 85°, NACA TN 3863, December, 1956.

20. Henderson, W. P.: The Longitudinal Aerodynamic Characteristics of a Swept-Back Wing-Body Combination With and Without End Plates at Mach Numbers from 0.40 to 0.93, NASA Technical Note D-389, May, 1960.

21. Roberts, S. C.: An Investigation of End Plates to Reduce the Drag of Planar Wings, Aerophysics Research Report No. 58, Mississippi State University Department of Aerophysics, January, 1966 (USAA VLABS Technical Report 65-79).

22. Ashley, H., and Landahl, M.: Aerodynamics of Wings and Bodies, Addison-Wesley, 1965, pp 208-220.

23. Blackwell, J. A., Jr.: Numerical Method for the Design of Warped Surfaces for Subsonic Wings With Arbitrary Planform, M.S. Thesis, University of Virginia, August, 1966.

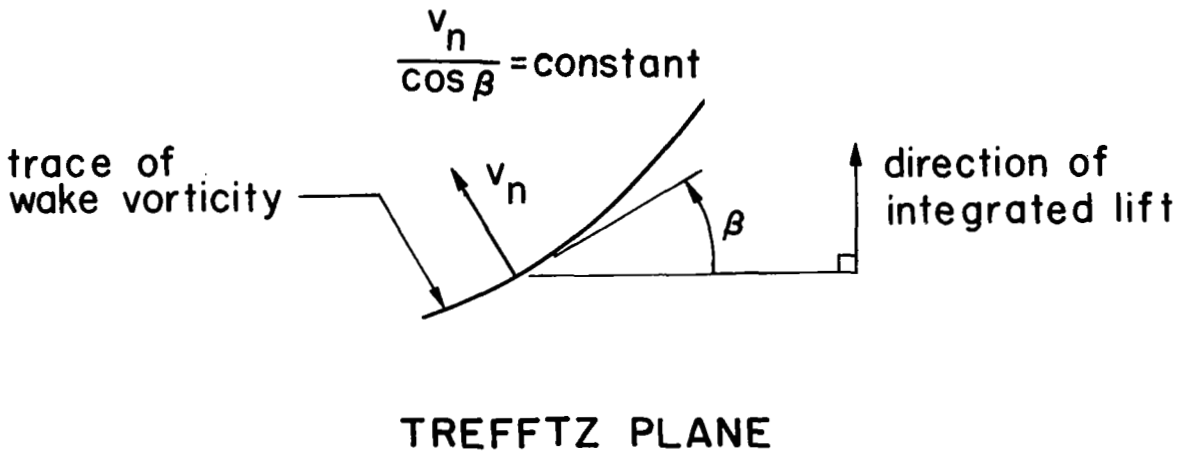

Figure 1. Munk's Minimum Induced Drag Criterion

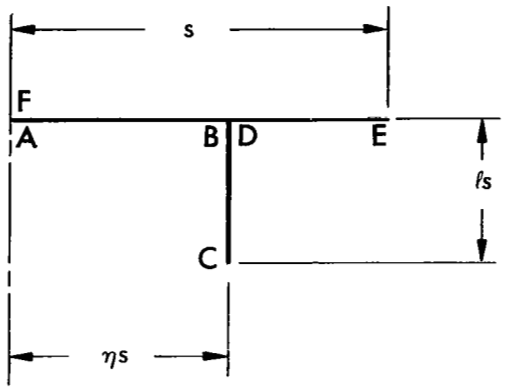

CONFIGURATION 1

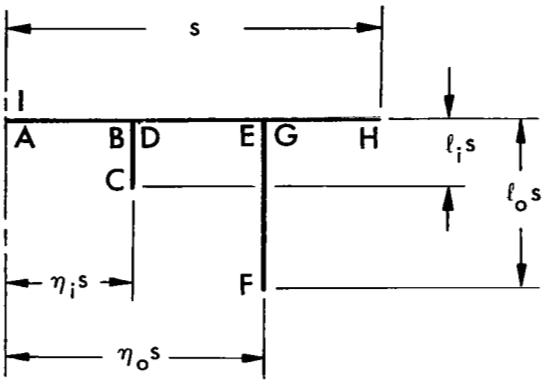

CONFIGURATION 2

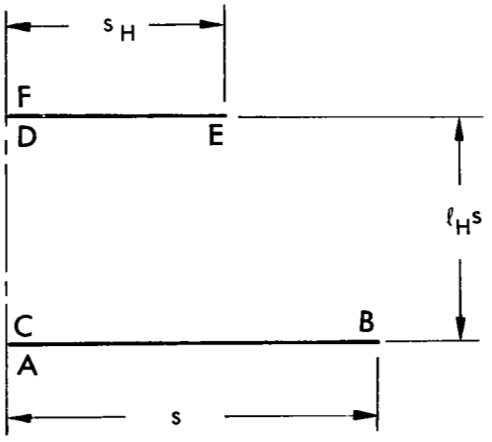

CONFIGURATION 3

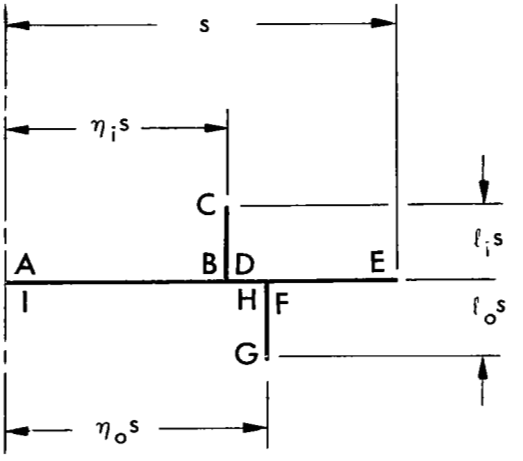

CONFIGURATION 4

Figure 2a. Configurations 1-4

Figure 2. Configurations Analyzed by Program 55VD

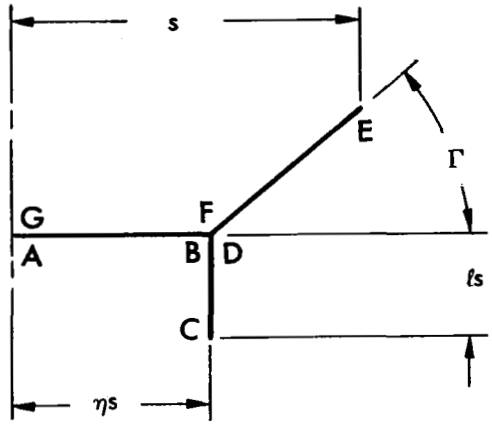

CONFIGURATION 5

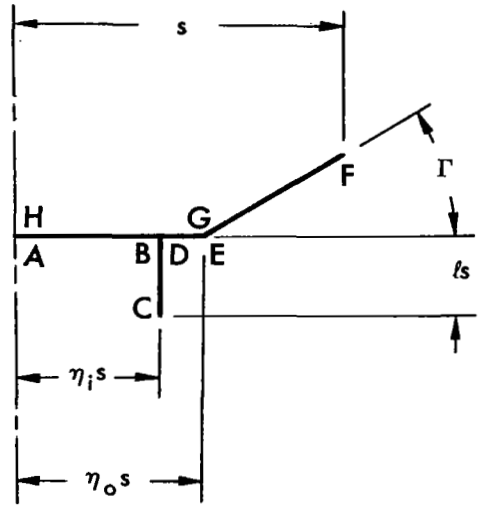

CONFIGURATION 6

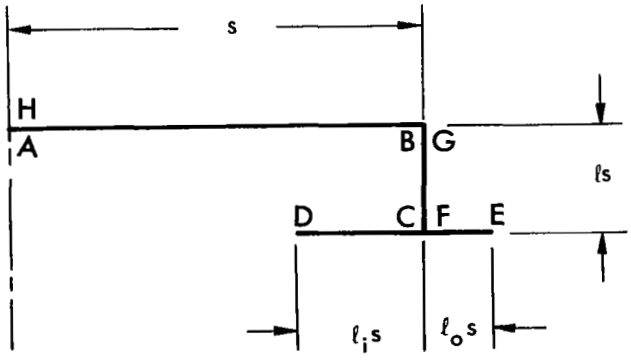

CONFIGURATION 7

Figure 2b. Configurations 5-7

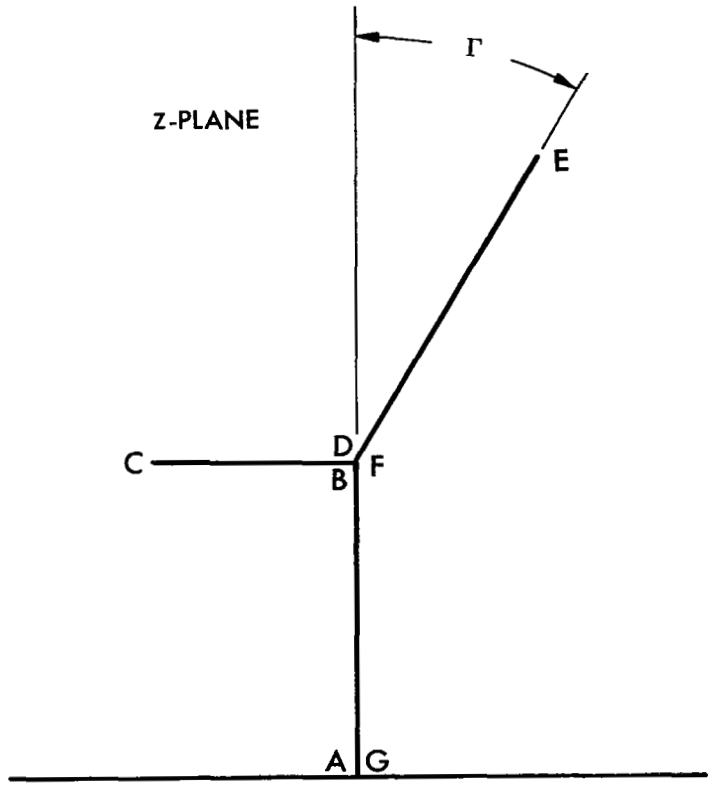

Figure 3a. Real Plane

$$\frac{dz}{d\zeta} = \frac{(\zeta\text{-}c)(\zeta\text{-}e)}{[(\zeta\text{-}a)(\zeta\text{-}b)(\zeta\text{-}g)]^{1/2}} (\zeta\text{-}d)^{\frac{\Gamma}{\pi}-\frac{1}{2}} (\zeta\text{-}f)^{-\frac{\Gamma}{\pi}}$$

ζ-PLANE

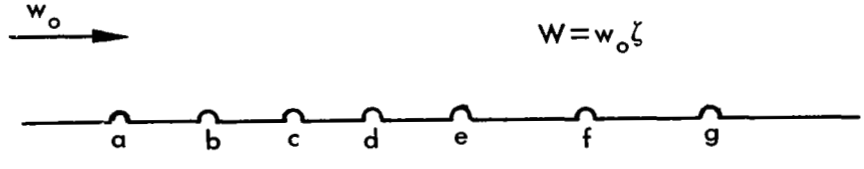

Figure 3b. Auxiliary Plane

Figure 3. Mapping Planes for Configuration 5

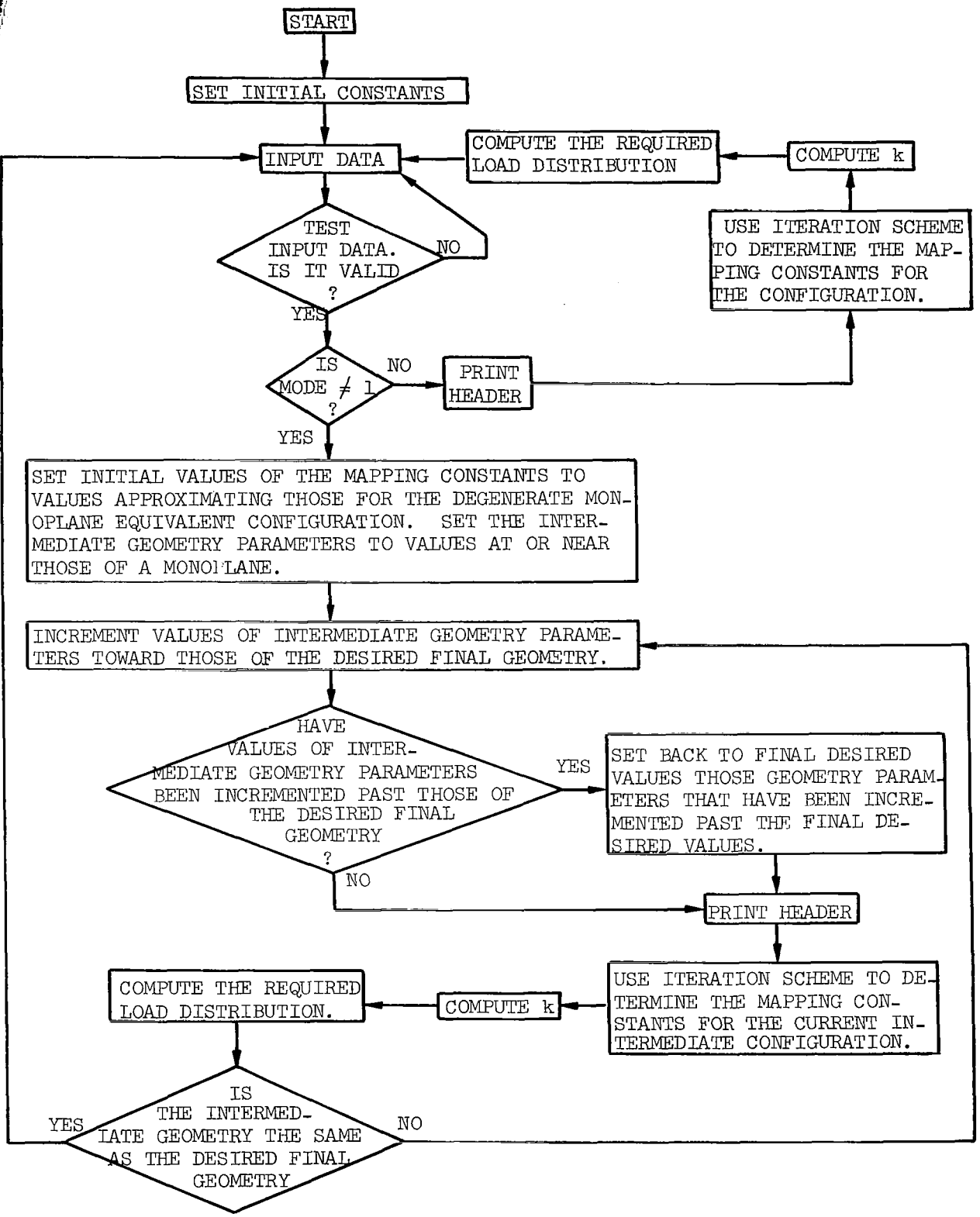

Figure 4. Overall Logical Flow of Computer Program 55VD

CONFIGURATION 1

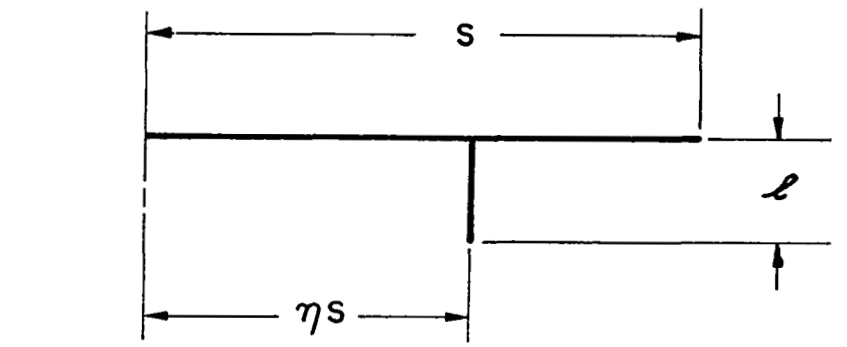

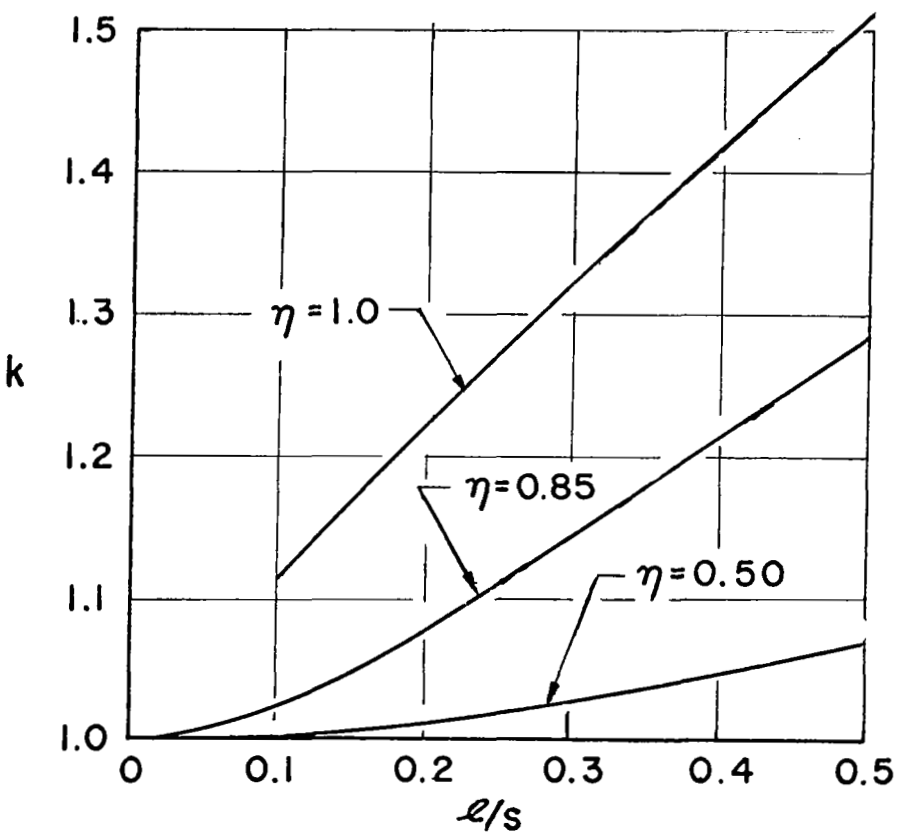

Figure 5. Induced Drag Efficiency at Minimum Induced Drag for a Wing with Vertical Fences

CONFIGURATION 3

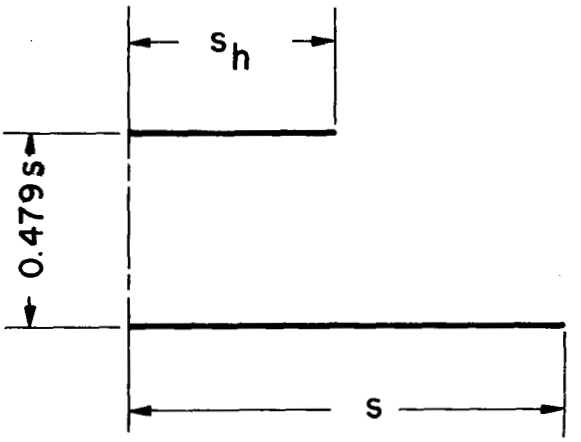

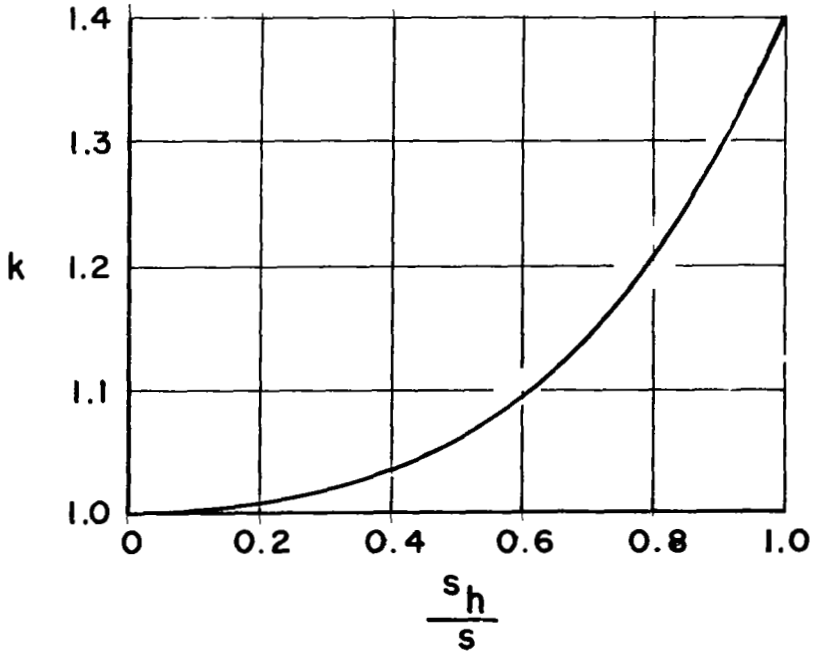

Figure 6. Induced Drag Efficiency at Minimum Induced Drag for a Biplane

CONFIGURATION 2

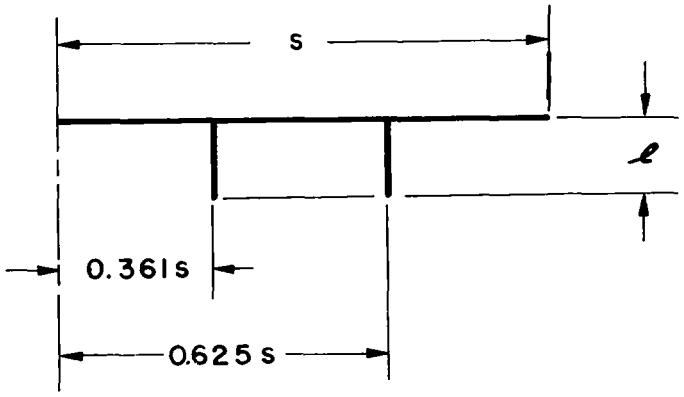

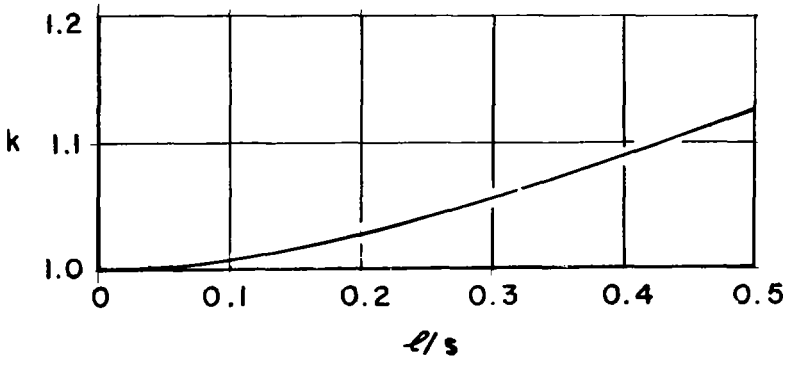

Figure 7. Induced Drag Efficiency at Minimum Induced Drag for a Wing with Two Vertical Fences

CONFIGURATION 4

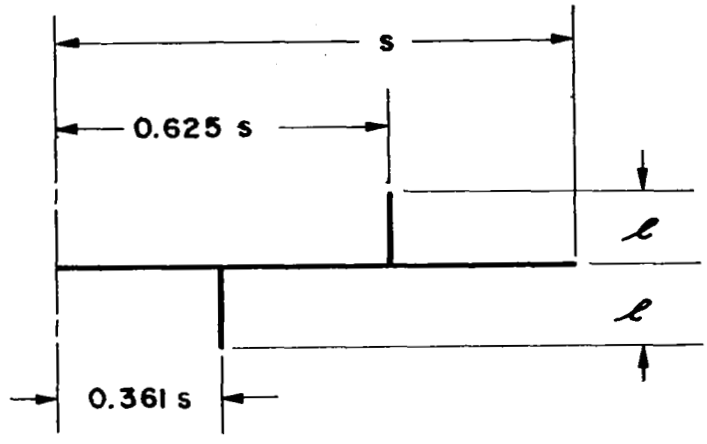

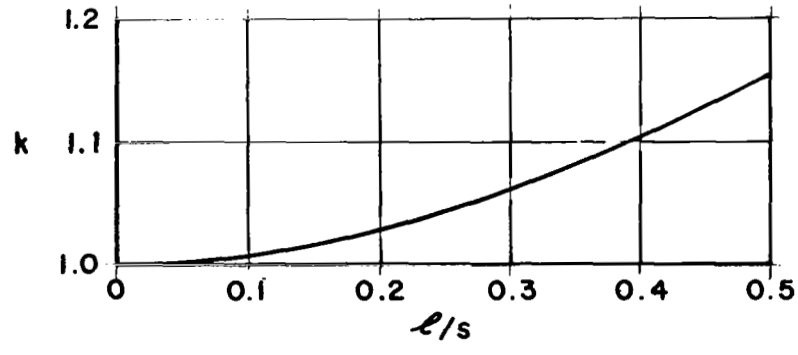

Figure 8. Induced Drag Efficiency at Minimum Induced Drag for a Wing with Vertical Fences Above and Below

CONFIGURATION 4

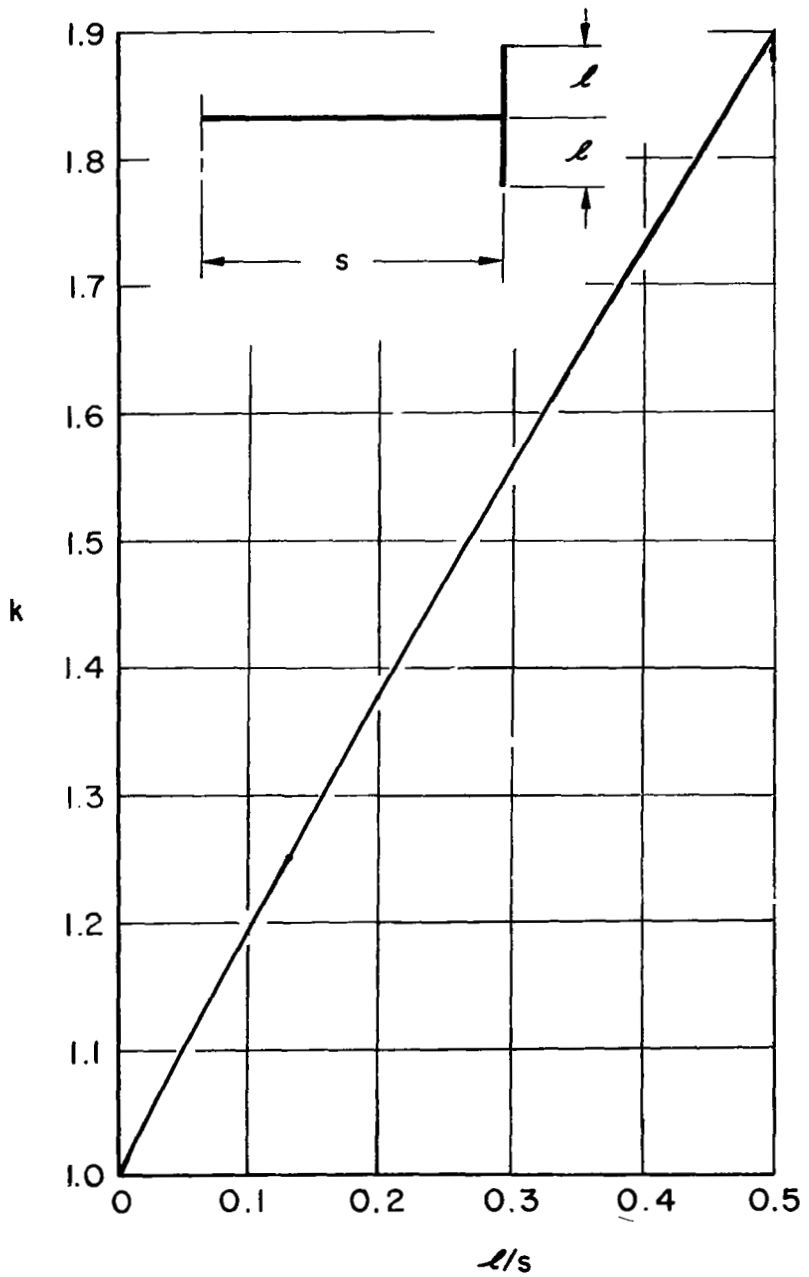

Figure 9. Induced Drag Efficiency at Minimum Induced Drag for a Wing with End Plates

CONFIGURATION 5 η=0.5, Γ=30°

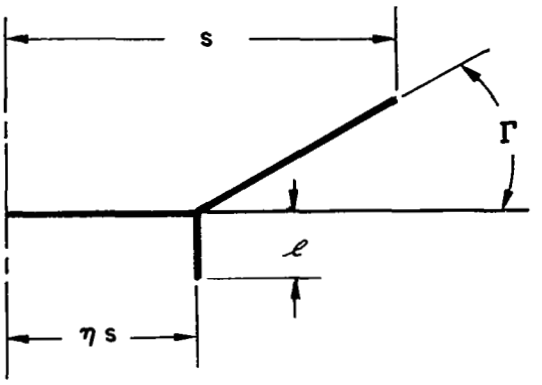

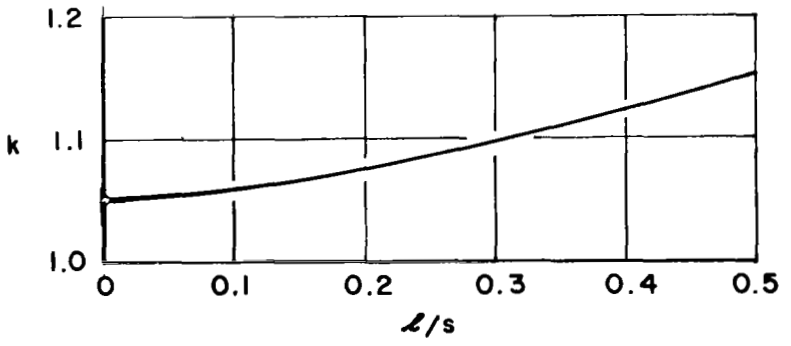

Figure 10. Induced Drag Efficiency at Minimum Induced Drag for a Wing with a Vertical Fence and Outboard Dihedral

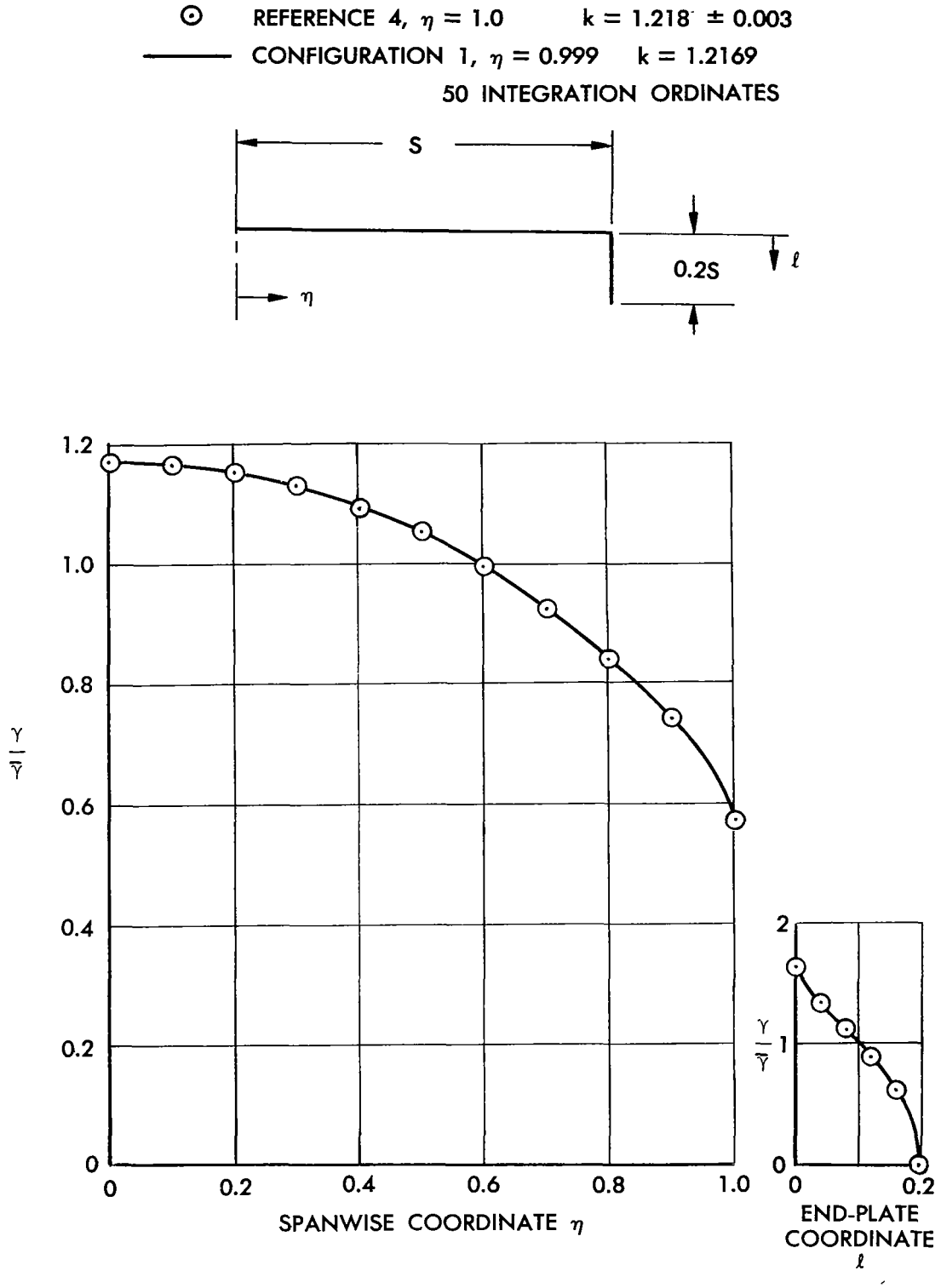

Figure 11. Loading for Minimum Induced Drag on a Wing with End Plates

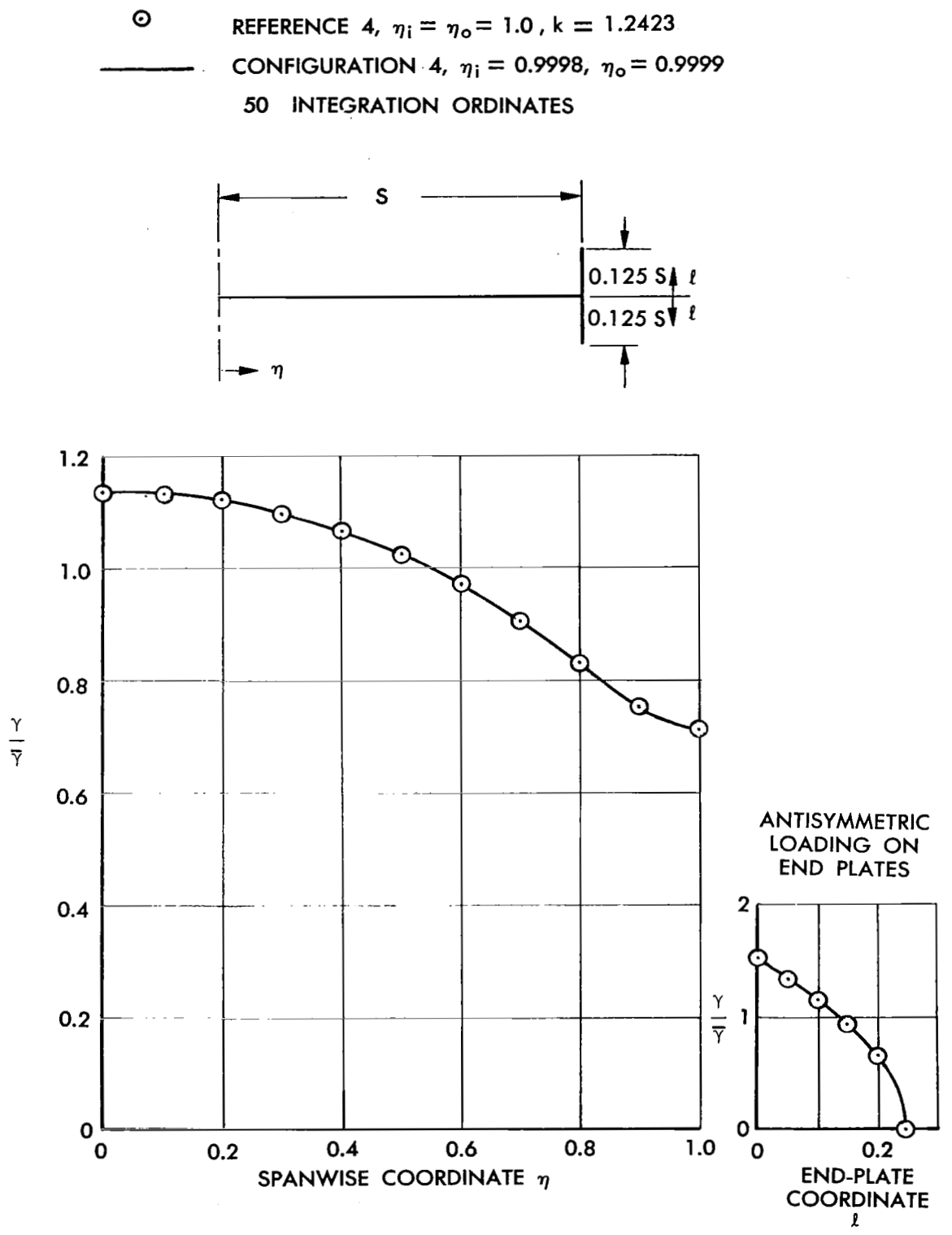

Figure 12. Loading for Minimum Induced Drag on a Wing with End Plates

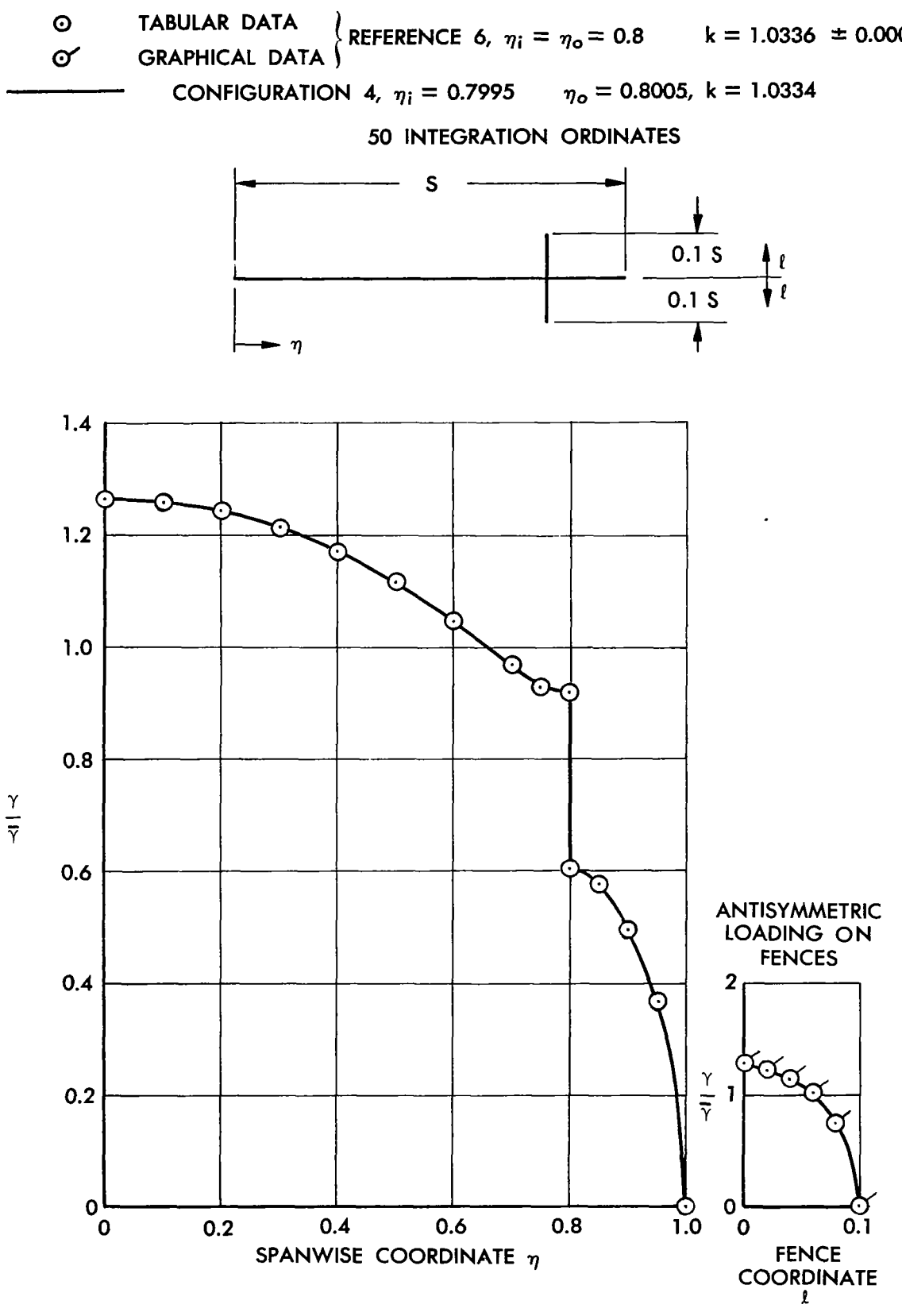

Figure 13. Loading for Minimum Induced Drag on a Wing with Vertical Fences

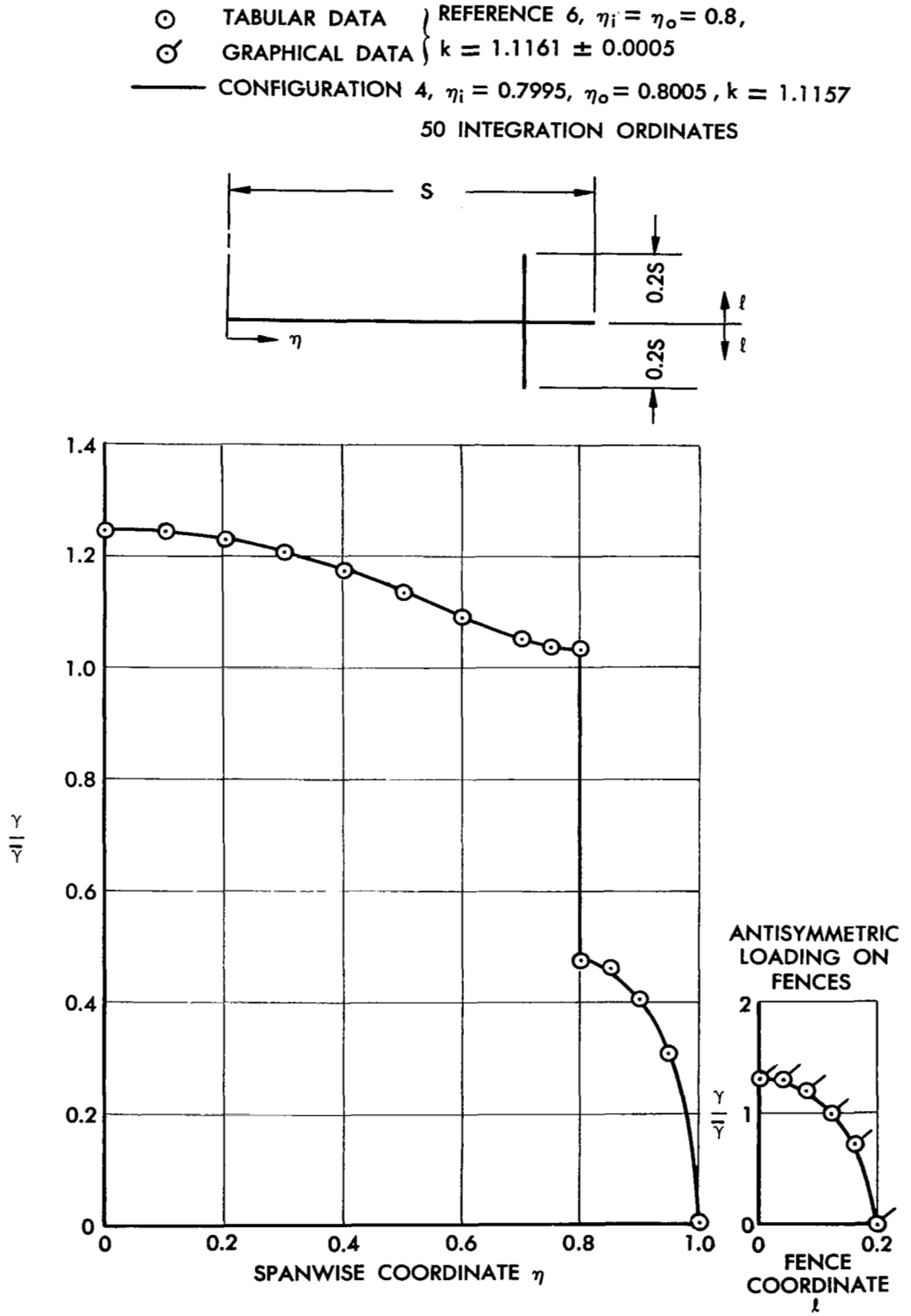

Figure 14. Loading for Minimum Induced Drag on a Wing with Vertical Fences

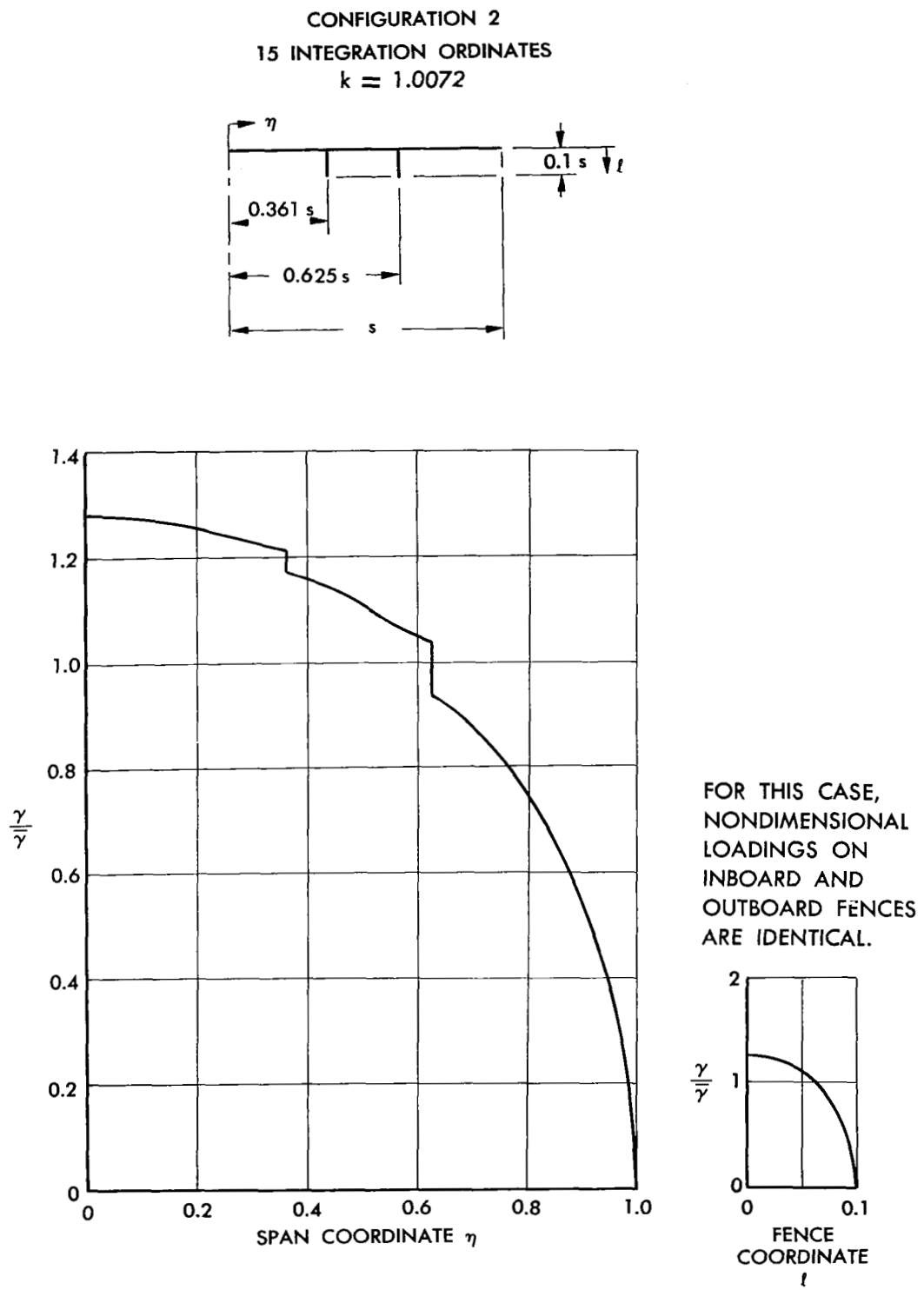

Figure 15. Loading for Minimum Induced Drag on a Wing with Two Vertical Fences

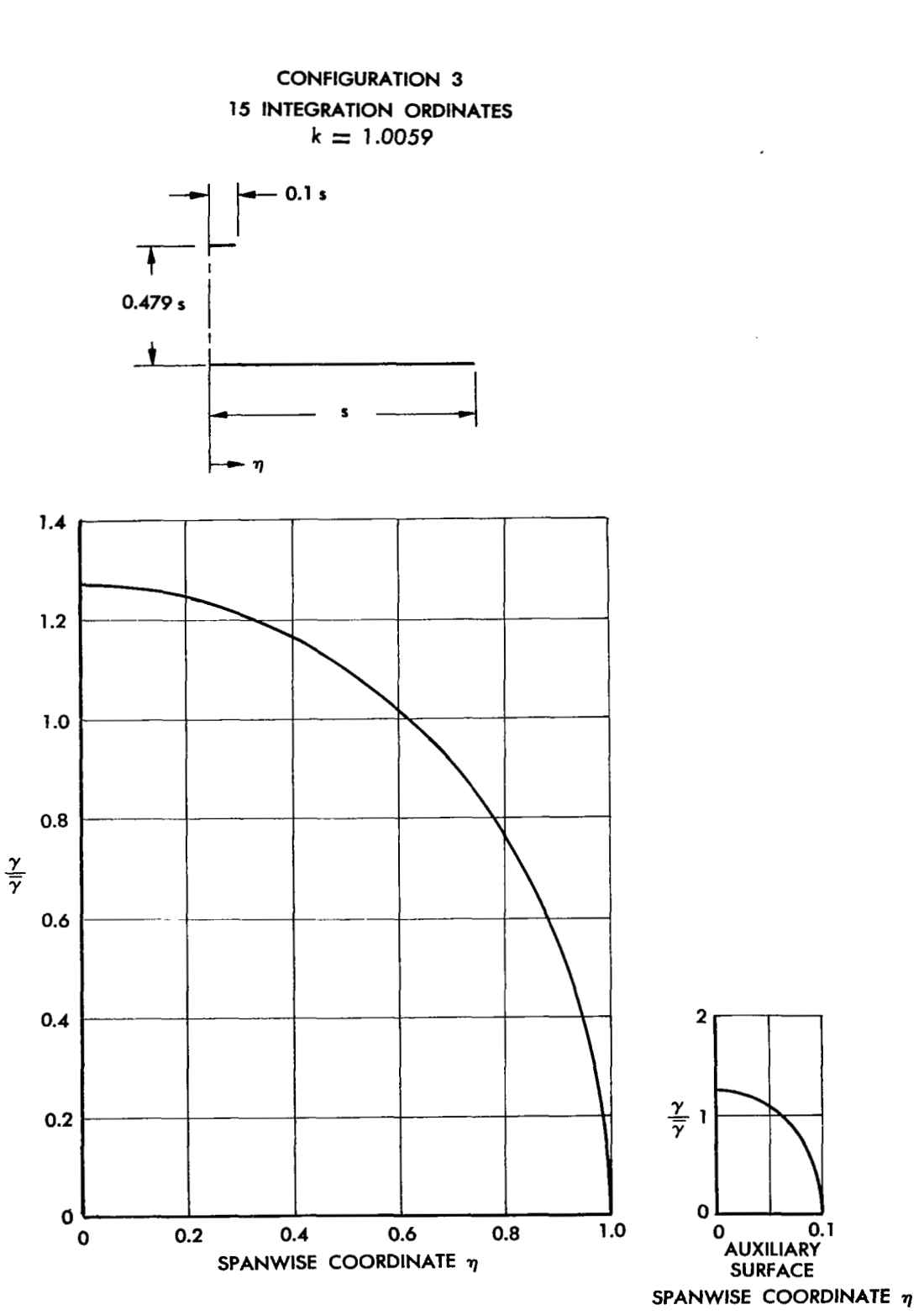

Figure 16. Loading for Minimum Induced Drag on a Biplane

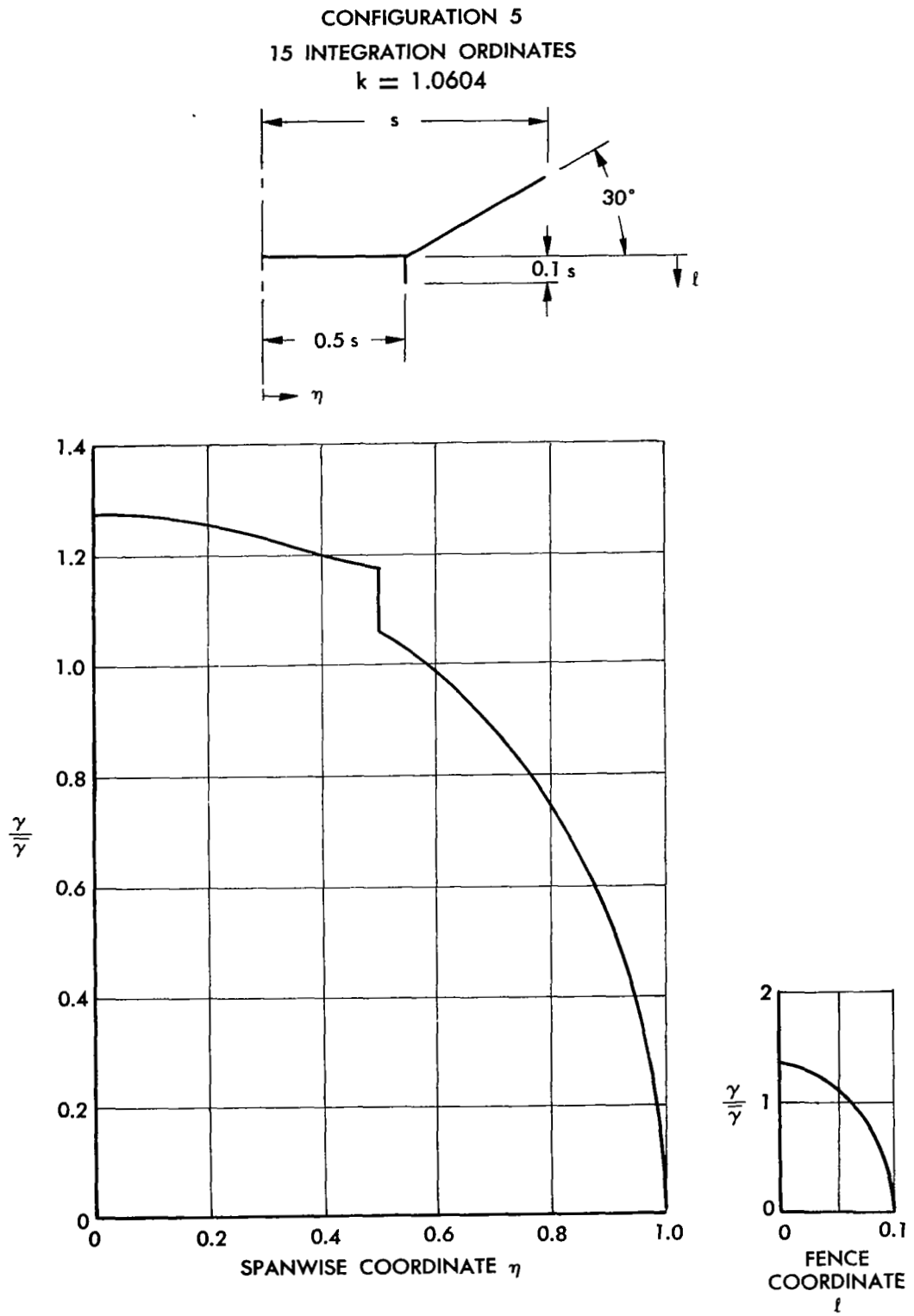

Figure 17. Loading for Minimum Induced Drag on a Wing with a Vertical Fence and Outboard Dihedral

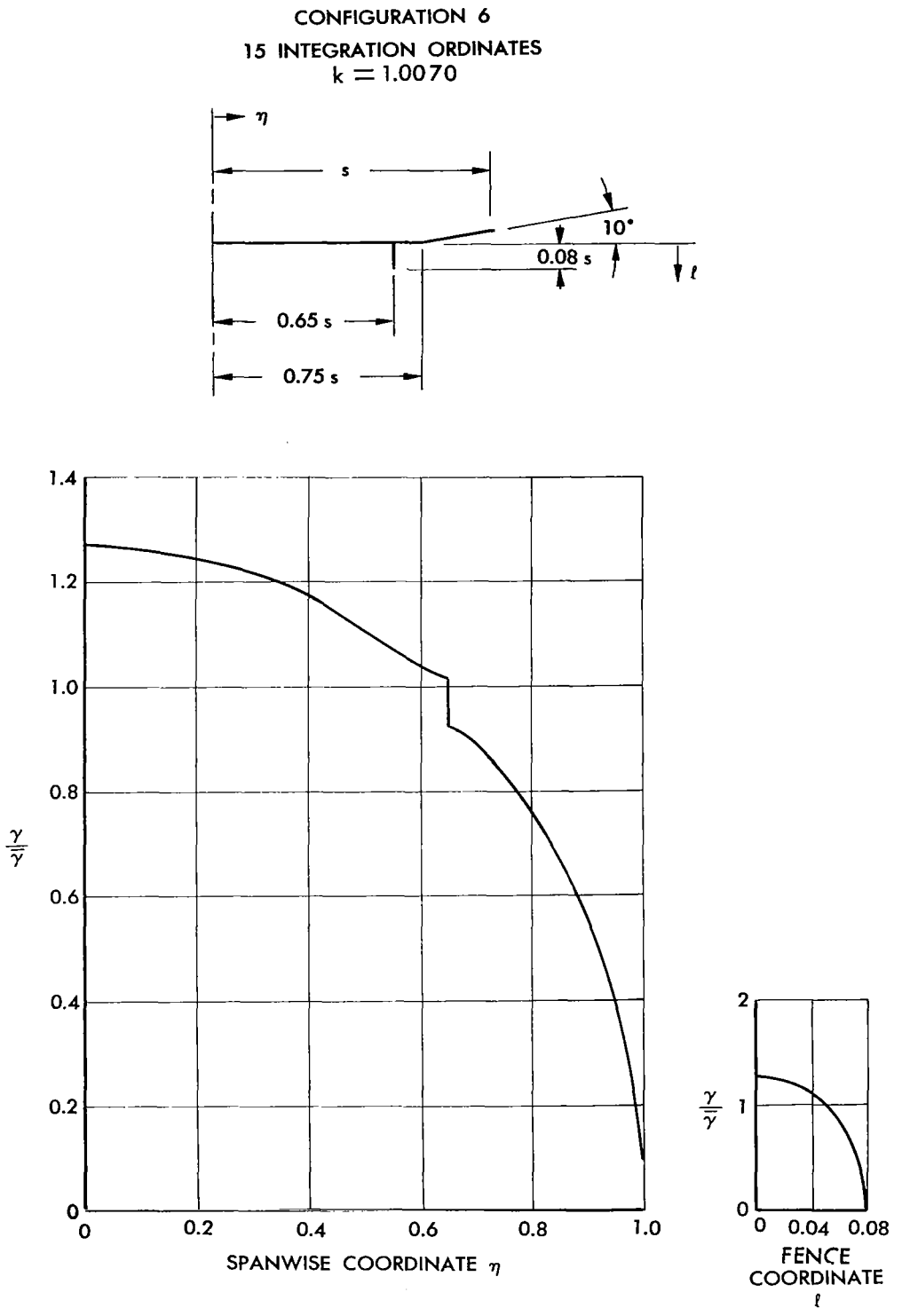

Figure 18. Loading for Minimum Induced Drag on a Wing with an Inboard Vertical Fence and Outboard Dihedral

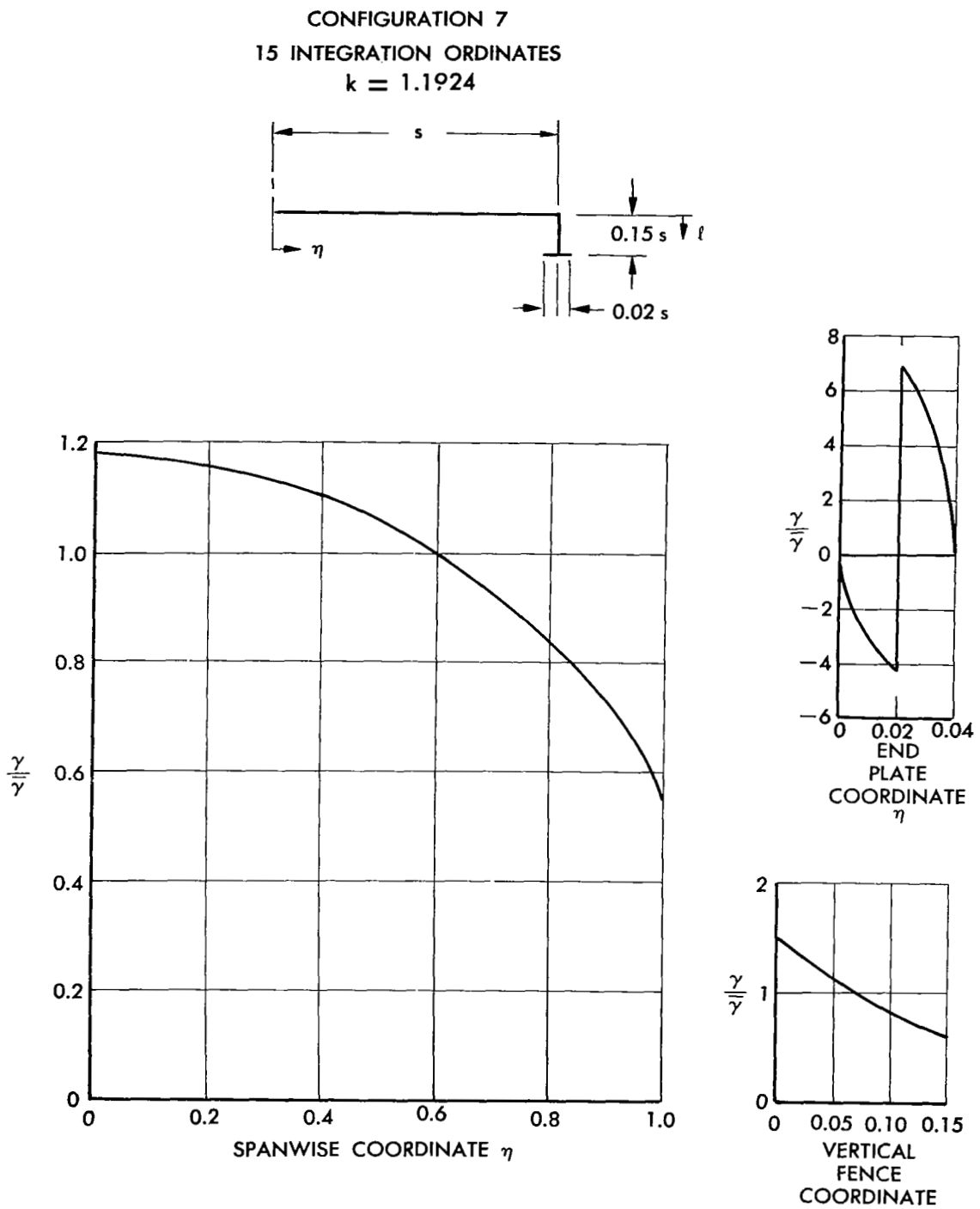

Figure 19. Loading for Minimum Induced Drag on a Wing with an End-Plated Vertical Fence at the Tip

NASA-Langley, 1968 — 1 CR-1218

"The aeronautical and space activities of the United States shall be conducted so as to contribute . . . to the expansion of human knowledge of phenomena in the atmosphere and space. The Administration shall provide for the widest practicable and appropriate dissemination of information concerning its activities and the results thereof."

—NATIONAL AERONAUTICS AND SPACE ACT OF 1958

NASA SCIENTIFIC AND TECHNICAL PUBLICATIONS

TECHNICAL REPORTS: Scientific and technical information considered important, complete, and a lasting contribution to existing knowledge.

TECHNICAL NOTES: Information less broad in scope but nevertheless of importance as a contribution to existing knowledge.

TECHNICAL MEMORANDUMS: Information receiving limited distribution because of preliminary data, security classification, or other reasons.

CONTRACTOR REPORTS: Scientific and technical information generated under a NASA contract or grant and considered an important contribution to existing knowledge.

TECHNICAL TRANSLATIONS: Information published in a foreign language considered to merit NASA distribution in English.

SPECIAL PUBLICATIONS: Information derived from or of value to NASA activities. Publications include conference proceedings, monographs, data compilations, handbooks, sourcebooks, and special bibliographies.

TECHNOLOGY UTILIZATION PUBLICATIONS: Information on technology used by NASA that may be of particular interest in commercial and other non-aerospace applications. Publications include Tech Briefs, Technology Utilization Reports and Notes, and Technology Surveys.

Details on the availability of these publications may be obtained from:

SCIENTIFIC AND TECHNICAL INFORMATION DIVISION

NATIONAL AERONAUTICS AND SPACE ADMINISTRATION

Washington, D.C. 20546